

Universal Scaling in Transient Creep

Dag Kristian Dysthe,^{*} Yuri Podladchikov,[†] Francois Renard,[‡] Jens Feder, and Bjørn Jamtveit

Physics of Geological Processes, Postbox 1048 Blindern, N-0316 Oslo, Norway

(Received 30 April 2002; published 20 November 2002)

We present experimental evidence that pressure solution creep does not establish a steady-state interface microstructure as previously thought. Conversely, pressure solution controlled strain and the characteristic length scale of interface microstructures grow as the cubic root of time. Transient creep with the same scaling is known in metallurgy (Andrade creep). The apparent universal scaling of pressure solution transient creep is explained using an analogy with spinodal dewetting.

DOI: 10.1103/PhysRevLett.89.246102

PACS numbers: 68.08.-p, 68.15.+e, 68.37.-d, 68.55.-a

Introduction.—When aggregates of small grains are pressed together in the presence of small amounts of solvent the aggregate compacts and the grains tend to stick together. This happens to salt and sugar in humid air, and to sediments when buried in the Earth's crust. Stress concentration at the grain contacts cause local dissolution, diffusion of the dissolved material out of the interface, and deposition on the less stressed faces of the grains [1]. This process, in geology known as pressure solution creep, plays a central role during compaction of sedimentary basins [1,2], during tectonic deformation of the Earth's crust [3], in strengthening of active fault gouges following earthquakes [4,5] and in ceramics [6]. Experimental data on pressure solution creep has so far not been sufficiently accurate to understand the transient processes at the grain scale.

Predictions of pressure solution creep rates from geological data and theoretical models vary by many orders of magnitude [7] because the fundamental processes are not yet fully understood. Pressure solution creep is a macroscopic phenomenon that depends on the slow interface dynamics at the grain-grain contact. Because of the slow creep at each interface (estimated range is from 100 nm/h for NaCl to 1 nm/yr for quartz at room temperature), experiments have been performed on aggregates (thus multiplying the number of contributing interfaces) or with low resolution relative to the measured strain rate. Experiments on aggregates involve other processes as well and are not readily deconvoluted to yield information on single interface dynamics. Detection of slow transient processes also requires experimentally a large dynamic range in time and in space.

Experiments.—We have developed two capacitance dilatometers to measure pressure solution creep rates and a method to obtain quantitative data on the interface structure for varying conditions and experiment duration (see Fig. 1). In our instruments inert indenters are pressed against the surface of single crystals of sodium chloride in the presence of saturated brine. The brine is sealed in the sample holders by hexadecane. Sodium chloride has for many years been used as a model material to study pressure solution creep [12–14]. One dilatometer was

built for long time stability, the second for measuring short time responses. The high sensitivity and stability of the dilatometers have proved necessary in order to detect the slow changes in indentation rates reported here.

In the dilatometers the samples are placed on sapphire flats inside hollow cylinders. Inert indenters are pressed by a piston against the sample surface in the presence of a few microliters of saturated brine. A capacitor is formed by the gold plated top of the hollow cylinder and the gold plated disk resting on the piston. When the indentors indent the sample the gap between the electrodes (approximately 100 μm) is reduced and the capacitance increases. In the single capacitance dilatometer [8,9] (left panel in Fig. 1) the capacitance is measured by a capacitance bridge and a lock-in amplifier. In the differential dilatometer [10] (middle panel in Fig. 1) the two capacitances constitute the two sides of the bridge and the difference ($C_1 - C_2$) is measured. The differential dilatometer has two nominally equal sets of samples, indentors, and pistons in order to cancel out the elastic and the plastic response of the system due to changes in dead-weight. The only difference between the two sides is the presence/absence of brine in the lower/upper part; thus any measured response ($C_1 - C_2$) is due only to pressure solution.

To avoid differential thermal dilatation of the components or changes in the solubility of the brine, the instruments have three stage thermal controls consisting of an air-conditioned room, thermalized circulating oil bath, and a feedback loop with a thermistor and a Peltier element. The root mean square thermal fluctuations are 2×10^{-7} K and 2×10^{-5} K over periods of weeks for the single and differential capacitance dilatometers, respectively. The single capacitance dilatometer has a sensitivity of 0.1 \AA and a stability of 10 nm over periods of weeks and can accurately measure indentation rates lower than 1 $\text{\AA}/\text{h}$. The differential dilatometer has a sensitivity of 1 \AA and a stability of 10 nm over 10 h.

The device for surface structure experiments [11] is shown in the right panel of Fig. 1. The sample is contained in a small glass cylinder glued to a glass base. The indenter, a gold wire mesh, is placed on top of the sample

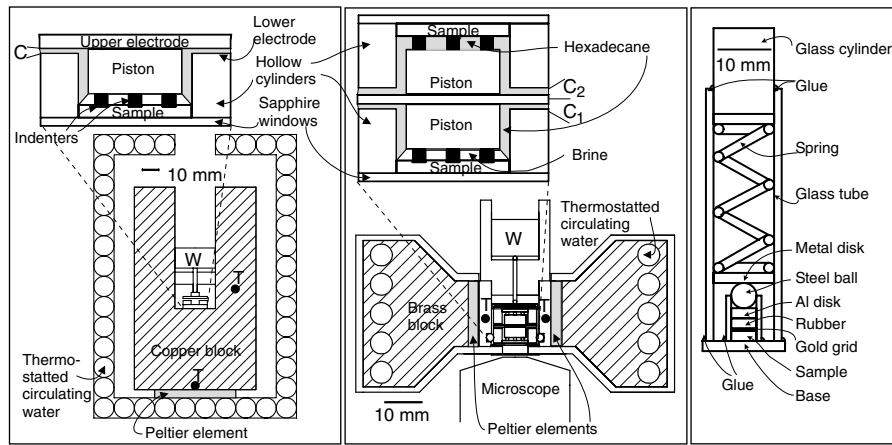


FIG. 1. Experimental devices. Left panel: Single capacitance dilatometer for long time stability [8,9]. Middle panel: Differential capacitance dilatometer for short term response [10]. Right panel: Experimental device for structure experiments [11]. The dilatometers are based on the principle that indentation of indentors into the sample cause the upper electrode to approach the lower electrode (top surface of the hollow cylinder) and the capacitance increases. High resolution requires stable temperature assured by the thermal control systems shown below with thermostatted fluid and Peltier elements. The device to the right is conceived for keeping a constant load from the indenting gold grid on the sample in a closed system and for cheaply performing many parallel experiments (30 devices were built).

with $4 \mu\text{l}$ saturated brine present and sealed off by hexadecane. The force on the indentors is applied by a spring that is contained in an outer glass tube and acted upon by a glass cylinder. The spring is compressed with the desired deadweight while the glue between the glass cylinder and glass tube is hardened with blue light. The entire device is thereby sealed to avoid evaporation of the hexadecane. The device can be moved and stored at the desired temperature and duration before the outer cylinder is broken and the sample is quickly removed and brine is flushed off with hexane. The sample surface with indented regions is imaged by white light interferometer (WLI) micrography (Wyko 2000 Surface Profiler from Veeco). This is done by a microscope with a reference arm creating interference fringes with maximum intensity at equal optical path lengths of the imaging beam and reference beam. By vertical movement of the sample and simultaneous image capturing the interference intensity envelope and thereby the relative height of the imaged surface at each pixel is determined with a resolution of 3 nm . The horizontal resolution depends on the lens used and with the highest magnification it is at the diffraction limit of about $0.5 \mu\text{m}$. The height “images” (intensity/color representing height) are treated by low pass Fourier filters with varying cutoff wavelengths. The filtered images are compared to the raw image and the filtered image with the largest cutoff wavelength that represents the main features of the unfiltered image is the optimum fit. The cutoff wavelength of the optimum fit image is called the characteristic length scale. The gold mesh indenter surface has a characteristic length scale of $1.7 \mu\text{m}$.

Results.—A “flat” surface always has a long range (waviness) and a short range (roughness) structure. When flat indentors are brought in contact with a flat surface there will only be a few contact points. As these points

dissolve by pressure solution, the area of contact increases until the whole surface of the indentors appears to be in contact with the crystal. In our rate experiments (see Figs. 1 and 2) the load applied by a deadweight was constant and a constant apparent contact surface was established after an initial period of approximately 10 h. From that time on the nominal normal stress applied by the indentors was constant. According to existing theories of pressure solution creep [1,6,7,12,15] one would expect a constant rate of indentation. However, as shown in Fig. 2, we observed that the indentation rate decreases slowly with time. The indentation as a function of time (after the constant nominal contact area was reached) follows a power law with an exponent, $\alpha = 1/3$ over 1.5

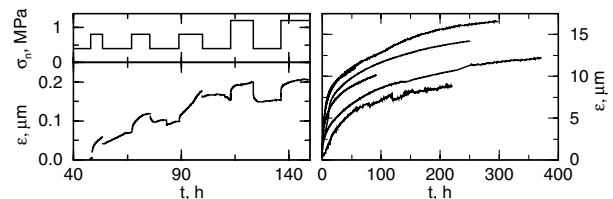


FIG. 2. Indentation-time data. Right panel: Indentation, ε , versus time, t , by pressure solution creep of gold wires into sodium chloride under constant load of 4 MPa measured by the single capacitance dilatometer. The different curves represent different samples with different surface treatment (ground, polished, cleaved) and brine volumes. The first 10 h the indentation rate varies among the samples due to different nominal contact area because of variation in sample waviness and roughness. Left panel: Indentation, ε , versus time, t (lower curve), by pressure solution creep of glass cylinders into sodium chloride under varying load (upper curve). Each time the load is increased the indentation speed immediately increases and subsequently slows down.

to 3 orders of magnitude. An increase of the interval defining this power law behavior would require either yearlong experiments or high resolution data for short times. The last option was inhibited by the initial change in area of contact. We observed, however, that every time the load was increased the indentation rate increased enormously and then slowly decreased with time again. This behavior suggests that the time-dependent process responsible for the decrease in indentation rate is “re-initialized” by an increase in normal stress at the contact. We therefore conducted experiments with a cyclic change in the load on the indenter. To improve the sensitivity immediately after a change in load, a differential dilatometer was built (see Fig. 1). Figure 2 shows the raw data from both experiments — with constant and varying load. The two sets of data are also represented in Fig. 3 by the logarithm of the indentation after a load increase as a function of the logarithm of the time after the load increase. The black curves (constant load) start off with a steep slope due to the change in contact area and tend towards a slope of about 0.3 after a constant contact area was established. The red curves (varying load) have a slope close to 1 up to approximately 1 min after the load change and cross over to a slope of approximately 0.3, coinciding and overlapping with the slope of the long time constant load experiments.

Since the macroscopic parameters of the experiment (temperature, load, contact area, saturation of the brine) were held constant in time the change in pressure solution creep rate must be related to some change in the contact interface itself. We performed a series of indentation

experiments (see Fig. 3) to systematically study the evolution of the interface structure during pressure solution creep. The experiments were performed at temperatures of 3, 23, 60, and 90 °C and normal stresses of 0.2, 2, and 20 MPa. After 1, 10, 100, and 1000 h, the indenter was removed and the pressure dissolved surface was imaged by WLI. From the images we obtained a characteristic length scale of the interface structure for each experiment. At small loads, low temperatures, and short experiment durations the indentors left no measurable imprints or the measured surface structure had a length scale approximately equal to the unindented surface. For experiments where the interface structure was clearly distinguishable from the unindented surface we found that the characteristic length scale of the surface increased with increasing stress, temperature, and with the cube root of time (Fig. 3).

Discussion.—Grains that have undergone pressure solution creep in Nature and during experiments are often found to have structured (as opposed to flat) interfaces. These structures depend on material parameters and pressure solution history. They include features such as fluid inclusions [16], fluid channels [16,17], grooves or corroded microcracks [7], dendritic contact regions [18], and negative crystal shapes [19]. The presence of grain boundary structures has long been recognized as important for the effectiveness of pressure solution creep [6,7,12,16–20]. The characteristic length scale of the contact island, d , is the key quantitative parameter. Different estimates of d yield orders of magnitude difference in predictions of strain rate, $d\varepsilon/dt$, through the scaling [7]

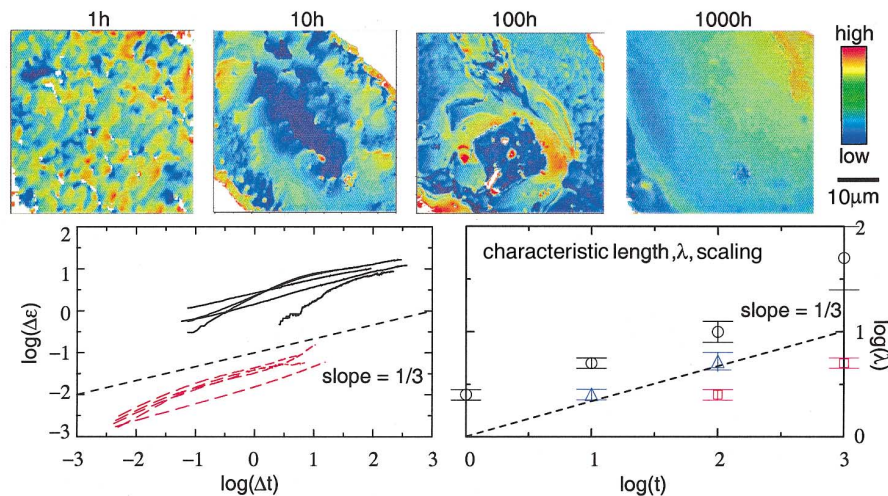


FIG. 3 (color). Evolution of the interface structure during pressure solution creep. Top panel: Experimental WLI micrographs for pressure solution creep at 20 MPa and 90 °C with varying duration of experiment. Image scale is the same in all pictures but vertical color code varies. The characteristic length scale increases until it reaches the dimension of the indenter (1000 h). Lower right panel: Logarithm of characteristic length scales vs logarithm of time for 20 MPa, 90 °C (circles), 2 MPa, 23 °C (squares), and 2 MPa, 60 °C (triangles). Each set of data has a slope of approximately 1/3. Lower left panel: Logarithm of the indentation after a load increase $\Delta\varepsilon = \varepsilon - \varepsilon_0$ as a function of logarithm of time (in minutes) after the load increase $\Delta t = t - t_0$. Individual curves are from Fig. 2 using $\varepsilon_0 = t_0 = 0$ for the single load experiments (black curves) and ε_0 and t_0 the indentation and time at load increase for the varying load experiments (red curves). One observes that apart from the first minute after a load increase both sets of data have a slope of approximately 1/3.

$d\varepsilon/dt \sim d^{-2}$. The length scale parameter, d , is believed (due to lack of time resolved experimental data) to be constant over time. The only exception is one *in situ* experiment which indicates that grain boundary fluid inclusions disappear with time [17] and the data presented here. The effect on creep behavior is dramatic: If d is a constant the strain is proportional to time, $\varepsilon \sim t$, and strain rate is constant. If the microstructure and d do evolve with time, i.e., in the simplest power law form $d \sim t^\alpha$, the corresponding strain will scale as $\varepsilon \sim t^{1-2\alpha}$. This transient creep regime continues until the length scale, d , reaches the size of the grain contact (at 1000 h, 90 °C in Fig. 3). Quantifying the scaling of characteristic length scales is experimentally difficult and recently an active area of research. It has recently been recognized that liquid films thinner than about 1 μm are often unstable and spontaneously develop various morphologies through processes similar to spinodal decomposition. In binary mixtures spinodal decomposition refers to the demixing as the system becomes unstable and moves along a cusp-like curve (spinode) towards phase separation [21]. It is well known that, for spinodal decomposition of mixtures, the characteristic scale of emerging phases coarsens with the cube root of time, $\alpha = 1/3$, which has also been confirmed for so-called spinodal dewetting of thin fluid films. It was furthermore shown by video microscopy [22] and numerical simulation [23] that a thin fluid film squeezed between solid surfaces follows the generic behavior of liquid films and spontaneously forms pockets of trapped liquid that coarsen with time. Assuming that the presence of dissolution does not alter the scaling behavior (the dissolution of the solid may in fact accommodate the formation of fluid pockets) of the thin fluid film, coarsening with $d \sim t^{1/3}$ yields the observed strain hardening relation $\varepsilon \sim t^{1/3}$ (Fig. 3). We argue that this strain hardening is due to a process analogous of thin film squeezing explained by spinodal decomposition in binary mixtures which exhibits the same cubic root coarsening in time. More generally it is well known that creep of many materials (from soft metals to noncrystalline materials such as celluloid) at constant temperature and stress usually follows the relationship $\varepsilon = \varepsilon_0 + \beta t^{1/3} + \kappa t$, where ε_0 is the instantaneous plastic strain, $\beta t^{1/3}$ is the so-called Andrade creep [24,25], and κt is steady-state creep. Andrade creep has not been adequately explained [26], but it has been recognized that due to the general nature it must be determined by a universal effect reminiscent of critical point behavior [24,27]. The apparent universal scaling of both Andrade creep and pressure solution creep may suggest that these processes reflect the presence of a “critical state” with the same scaling behavior as spinodal decomposition.

We thank Paul Meakin and Torstein Jøssang for numerous discussions. The project has been supported by the Norwegian Research Council through the Fluid Rock

Interaction Strategic University Program (Grant No. 113354/420) and by the Centre of Advanced Study at The Norwegian Academy of Sciences, where all the authors were affiliated during the academic year 2000–2001.

*Electronic address: d.k.dysthe@fys.uio.no

†Geologisches Institut, ETH-Zürich, Sonneggstrasse 5, 8092 Zürich, Switzerland.

‡LGIT-CNRS-Observatoire, Université Joseph Fourier, Grenoble F-38041, France.

- [1] P. K. Weyl, *J. Geophys. Res.* **69**, 2001 (1959).
- [2] M. T. Heald, *J. Geol.* **14**, 16 (1956).
- [3] S. Schwartz and B. Stöckert, *Tectonophysics* **255**, 203 (1996).
- [4] F. Renard, J. P. Gratier, and B. Jamtveit, *J. Struct. Geol.* **22**, 1395 (2000).
- [5] S. A. Miller, Y. Ben-Zion, and J. P. Burg, *J. Geophys. Res.* **104**, 10 621 (1999).
- [6] R. Raj, *J. Geophys. Res.* **87**, 4731 (1982).
- [7] S. W. J. denBrok, *Geology* **26**, 915 (1998).
- [8] T. H. Johansen, J. Feder, and T. Jøssang, *Rev. Sci. Instrum.* **57**, 1168 (1986).
- [9] D. K. Dysthe *et al.* (to be published).
- [10] D. K. Dysthe, F. Renard, J. G. Feder, and B. Jamtveit (to be published).
- [11] D. K. Dysthe, Y. Poladchikov, and B. Jamtveit (to be published).
- [12] C. J. Spiers *et al.*, in *Experimental Determination of Constitutive Parameters Governing Creep of Rocksalt by Pressure Solution*, Geological Society Special Publication Vol. 54, edited by R. J. Knipe and E. H. Rutter (The Geological Society, London, 1990), pp. 215–227.
- [13] J. L. Urai, C. J. Spiers, H. J. Zwart, and G. S. Lister, *Nature (London)* **324**, 554 (1986).
- [14] F. Renard *et al.*, *Geophys. Res. Lett.* **25**, 1295 (2001).
- [15] M. S. Paterson, *Rev. Geophys. Space Phys.* **11**, 355 (1973).
- [16] S. W. J. denBrok and C. J. Spiers, *J. Geol. Soc.* **148**, 541 (1991).
- [17] P. M. Schutjens and C. S. Spiers, *Oil Gas Sci. Tech.* **54**, 729 (1999).
- [18] S. H. Hickman and B. Evans, *J. Geol. Soc. (London)* **148**, 549 (1991).
- [19] A. J. Gratz, S. Manne, and P. K. Hatsma, *Science* **251**, 1343 (1991).
- [20] A. J. Gratz, *Geology* **19**, 901 (1991).
- [21] S. Herminghaus *et al.*, *Science* **282**, 916 (1998).
- [22] F. Mugele and M. Salmeron, *Phys. Rev. Lett.* **84**, 5796 (2000).
- [23] S. Zilberman *et al.*, *Phys. Rev. E* **63**, 055103 (2001).
- [24] E. N. daC. Andrade, *Proc. R. Soc. London A* **84**, 1 (1910).
- [25] A. H. Cottrell, *Philos. Mag. Lett.* **73**, 35 (1996).
- [26] F. R. N. Nabarro, *Theory of Crystal Dislocations* (Clarendon, Oxford, 1967).
- [27] D. C. Chrzan and M. J. Mills, *Phys. Rev. Lett.* **69**, 2795 (1992).